

# Scanning Tunneling Microscopy of Carbon Surfaces: Relationships between Electrode Kinetics, Capacitance, and Morphology for Glassy Carbon Electrodes

Mark T. McDermott, Christie Allred McDermott, and Richard L. McCreery\*

Department of Chemistry, The Ohio State University, 120 West 18th Avenue, Columbus, Ohio 43210

Polished, fractured, heat-treated, and laser-activated glassy carbon (GC) surfaces were examined by scanning tunneling microscopy (STM) in ambient air. Polished electrodes, as well as those which were vacuum heat treated (VHT) or laser activated (25 mW/cm<sup>2</sup>) after being polished, were comparably smooth in 2.5- $\mu$ m STM scans, exhibiting root-mean-square roughness (RMSR) of  $\sim$ 4 nm. Fractured, unpolished surfaces were significantly rougher (RMSR  $\sim$ 20 nm) and exhibited numerous nodules with diameters in the range of 50–300 nm. Polished surfaces laser activated at high-power density (70 MW/cm<sup>2</sup>) showed unexpected features along polishing scratches, apparently caused by local melting. The heterogeneous electron-transfer rate constant ( $k^0$ , cm/s) and capacitance ( $C^0$ ,  $\mu$ F/cm<sup>2</sup>) were also determined for the STM-characterized surfaces. Although rougher surfaces generally exhibited higher  $C^0$ , major differences in  $k^0$  were observed for surfaces with similar roughness and appearance. The results are consistent with the dominance of surface cleanliness in the mechanism of laser activation. Combined with past results based on adsorption, the morphological data indicate that differences in surface roughness are unimportant for laser activation of Fe(CN)<sub>6</sub><sup>4-/3-</sup> kinetics. Furthermore, the STM images reveal morphological effects of laser activation and polishing which were not apparent from previous electrochemical results.

## INTRODUCTION

Effective applications of solid electrodes in analysis, synthesis, and energy conversion result in part from an understanding of electrode surface properties and their effects on electron transfer. Glassy carbon (GC) is widely used as an electrode for analysis and as a substrate for modified electrodes largely because of its hardness, wide potential range, durability, and cost. However, the surface properties of a typical GC electrode are not thoroughly understood due to the variety of procedures used to prepare these electrodes and the large number of variables at the surface. The many procedures and associated effects on electrode kinetics and capacitance have been reviewed recently.<sup>1</sup> Because these surfaces are not well-defined, the major factors which determine electrochemical behavior have not been completely determined. The relationship between surface structural variables of GC and electrochemical phenomena such as heterogeneous electron-transfer kinetics and differential capacitance is the subject of this report.

Surface properties of carbon electrodes which affect electrochemical reactivity may be classified into four

categories: carbon microstructure, surface roughness, physisorbed impurities, and chemisorbed species, particularly oxides. The microstructural properties of various carbon materials are determined by their microcrystallite size, which will in turn determine the relative distribution of basal plane and edge plane regions at the surface. Graphite edge plane has been shown to differ greatly in electrochemical behavior from basal regions on ordered graphite surfaces.<sup>1-10</sup> However, the electrode activity will also be affected by the remaining three variables: roughness may determine the number of active sites, physisorbed impurities may cover or block active sites, and oxides may alter the mechanism of electron transfer altogether. Whether or not these variables are important to the behavior of a given electrode is determined by the electrode material and preparation history.

Our group and others have reported a number of surface preparations for GC electrodes. Pertinent examples of pretreatment methods are polishing,<sup>11-13</sup> laser activation,<sup>14-19</sup> vacuum heat treatment,<sup>13,20-22</sup> and exposure of the fresh bulk carbon by fracturing a GC rod in situ.<sup>17,18,23,24</sup> The purpose of these and other preparation schemes is to modify one or more of the GC surface variables mentioned above in order to affect electron-transfer rates of target redox systems. However, the effect of any particular electrode preparation procedure on the many GC surface factors remains unclear. For example, fracturing a GC electrode in solution should yield a surface relatively free of chemisorbed and physisorbed impurities with a microcrystallite size representative of the bulk carbon material. A polished surface, on the other hand,

(5) Bowling, R.; Packard, R.; McCreery, R. L. *J. Am. Chem. Soc.* 1989, 111, 1217-1223.

(6) Bowling, R.; Packard, R. T.; McCreery, R. L. *Langmuir* 1989, 5, 683-688.

(7) Rice, R. J.; McCreery, R. L. *Anal. Chem.* 1989, 61, 1637-1641.

(8) Robinson, R. S.; Sternitzke, K.; McDermott, M. T.; McCreery, R. L. *J. Electrochem. Soc.* 1991, 138, 2412-2418.

(9) McDermott, M. T.; Kneten, K.; McCreery, R. L. *J. Phys. Chem.* 1992, 96, 3124-3130.

(10) Kneten, K. R.; McCreery, R. L. *Anal. Chem.* 1992, 64, 2518-2524.

(11) Kamau, G. N.; Willis, W. S.; Rusling, J. F. *Anal. Chem.* 1985, 57, 545-551.

(12) Hu, I.; Karweik, D. H.; Kuwana, T. *J. Electroanal. Chem.* 1985, 188, 59-72.

(13) Wightman, R. M.; Deakin, M. R.; Kovach, P. M.; Kuhr, P. M.; Stutts, K. J. *J. Electrochem. Soc.* 1984, 131, 1578-1583.

(14) Poon, M.; McCreery, R. L. *Anal. Chem.* 1986, 58, 2745-2750.

(15) Poon, M.; McCreery, R. L. *Anal. Chem.* 1987, 59, 1615-1620.

(16) Poon, M.; McCreery, R. L.; Engstrom, R. *Anal. Chem.* 1988, 60, 1725-1730.

(17) Rice, R. J.; Pontikos, N.; McCreery, R. L. *J. Am. Chem. Soc.* 1990, 112, 4617-4622.

(18) Pontikos, N. M.; McCreery, R. L. *J. Electroanal. Chem.* 1992, 324, 229-242.

(19) Strein, T. G.; Ewing, A. G. *Anal. Chem.* 1991, 63, 194-198.

(20) Fagan, D. T.; Hu, I.; Kuwana, T. *Anal. Chem.* 1985, 57, 2759-2763.

(21) Stutts, K. J.; Kovach, P. M.; Kuhr, W. G.; Wightman, R. M. *Anal. Chem.* 1983, 55, 1632-1634.

(22) Hance, G. W.; Kuwana, T. *Anal. Chem.* 1987, 59, 131-134.

(23) Rice, R.; Allred, C.; McCreery, R. *J. Electroanal. Chem.* 1989, 263, 163-169.

(24) Allred, C. D.; McCreery, R. L. *Anal. Chem.* 1992, 64, 444-448.

\* Author to whom correspondence should be addressed.

(1) McCreery, R. L. In *Electroanal. Chemistry*; Bard, A. J., Ed.; Dekker: New York, 1991; Vol. 17, pp 221-374.

(2) Randin, J. P.; Yeager, E. *J. Electrochem. Soc.* 1971, 118, 711-714.

(3) Randin, J. P.; Yeager, E. *J. Electroanal. Chem.* 1972, 36, 257-276.

(4) Randin, J. P.; Yeager, E. *J. Electroanal. Chem.* 1975, 58, 313-322.

possesses a number of impurities and a microcrystalline structure quite different from that of the bulk carbon.<sup>18,23,24</sup> The fractured surface exhibits large heterogeneous electron-transfer rate constants ( $k^\circ$ ) for the ferro-/ferricyanide redox system compared to polished GC surfaces, but it is not clear whether this increase in rate is due to differences in microcrystallite size, microscopic roughness, surface cleanliness, or a combination of these variables.

There have been a number of surface techniques employed to study the surface structure of GC electrodes. Techniques commonly employed are X-ray photoelectron spectroscopy (XPS) and Auger electron spectroscopy (AES),<sup>11,12,20,21,25</sup> Raman spectroscopy,<sup>17,18,23</sup> surface-enhanced Raman spectroscopy (SERS),<sup>26,27</sup> and scanning electron microscopy (SEM).<sup>14,18,25,28</sup> Scanning tunneling microscopy (STM) has been used extensively to characterize highly ordered pyrolytic graphite (HOPG) electrodes at atomic resolution, including examination of the effects of electrochemical and chemical oxidation.<sup>30-32</sup> In several cases, defects on HOPG surfaces have been associated with increased chemical and electrochemical reactivity.<sup>9,31-35</sup> In an SEM study of GC by Bodalbhaj and Brajter-Toth,<sup>29</sup> the electrodeposition of copper at active sites was correlated with roughness and electron-transfer kinetics for  $\text{Fe}(\text{CN})_6^{4-/3-}$ . It was concluded that treatments which increase the density of copper nucleation sites also increase the electron-transfer rate. These techniques have been useful for understanding carbon electrode structure/reactivity relationships, but the structural models for GC surfaces remain incomplete at the scale below the SEM resolution limit of  $\sim 100 \text{ \AA}$ . A few reports of atomic scale STM of GC have appeared,<sup>36-38</sup> but in no case was the observed morphology related to electrochemical behavior. Furthermore, the variety of GC preparation procedures and test redox systems has made it difficult to compare the performance of different surfaces under otherwise identical conditions. Accordingly, the current effort involves the use of STM to provide surface morphological information about GC surfaces resulting from several pretreatment procedures and comparison of the electrode kinetics and capacitance of these surfaces. STM is particularly attractive because of high spatial resolution, especially in the vertical direction. In addition, SEM images of polished GC have been shown to be modified by the presence of a carbon microparticle layer.<sup>28</sup>

Electrochemically activated GC surfaces which had previously been polished have been imaged by two groups. Wang et al. compared surface roughness and topography imaged by STM for two different methods of electrochemical pretreatment (ECP)<sup>39</sup> and also used STM to investigate GC surface passivation due to phenol oxidation.<sup>40</sup> Freund et al. compared STM images and atomic force microscopy (AFM) images of

polished as well as electrochemically pretreated GC.<sup>41</sup> Both STM studies of electrochemically activated GC concluded that ECP resulted in a rougher surface relative to the initial polished surface. We report here an STM study of a number of other standard pretreatment procedures for GC electrodes. The surface morphology and relative roughness of conventionally polished, laser-irradiated, fractured, and vacuum heat treated GC surfaces are correlated with the electrochemical behavior as determined by the heterogeneous electron-transfer rate constant,  $k^\circ$ , for ferro-/ferricyanide and differential capacitance,  $C^\circ$ , for these surfaces. An essential component of our approach is observation of both STM images and electrochemical behavior on the *same* GC surface in order to reduce common problems with surface reproducibility. By comparing STM morphology and electrochemical activity for polished, laser-activated, fractured, and heat-treated GC, insights into electrode structure/reactivity relationships were obtained.

## EXPERIMENTAL SECTION

**Reagents.** All solutions were prepared with water obtained from a Nanopure II system (Barnstead, Dubuque, IA). Potassium ferrocyanide was used as received from Baker (Phillipsburg, NJ). Potassium chloride was used as received from Jenneil Chemical (Cincinnati, OH). Solutions of 1 mM  $\text{K}_4\text{Fe}(\text{CN})_6$  in 1 M KCl were made fresh daily and purged with purified argon prior to use.

**Electrode Preparation.** Glassy carbon (GC-20) working electrodes were obtained from Tokai and employed in one of three different mechanical shapes: a 3-mm-diameter GC rod, a GC disk cut from a 2-mm-thick plate and sanded to shape, and GC microelectrodes fabricated as described previously.<sup>18,24</sup> All electrodes (GC disks and microelectrodes) used in the correlation of roughness and morphology with electrochemical behavior (Figures 1-3 and Tables I-III) were manufactured from a single 2-mm-thick plate of Tokai GC-20. The high-resolution STM images of fractured GC in Figure 4 were taken on a 3-mm-diameter Tokai GC-20 rod because of the ease of mounting and lack of sample tilt compared to fractured GC microelectrodes. No differences were observed in the STM images between fractured 3-mm GC rods and fractured GC microelectrodes. The electrochemical cell was made of Teflon and was equipped with a quartz window through which the electrode could be laser irradiated. Disk electrode areas were defined by a viton o-ring, and microelectrode areas (ca.  $0.5 \times 0.5 \text{ mm}^2$ ) were defined by the exposed electrode face surrounded by a sheath of epoxy. The three-electrode cell was completed with a Bioanalytical Systems (West Lafayette, IN) Ag/AgCl (3 M NaCl) reference electrode and a platinum wire auxiliary electrode.

Polished electrodes were prepared by polishing with 600-grit silicon carbide paper followed by 1-, 0.3-, and 0.05- $\mu\text{m}$  alumina (Buehler, Lake Bluff, IL) slurries on Microcloth polishing cloth (Buehler). Slurries were prepared from dry alumina and Nanopure water. Polished electrodes were sonicated in Nanopure water for  $\sim 5$  min before placement in the electrochemical cell. Care was taken to ensure that a drop of water remained on the polished electrode during insertion into the Teflon cell until anlyte solution was added. In-situ laser activation of polished electrodes in Nanopure water was performed with a Nd:YAG laser (Model 580-10, Quantel) operating at 1064 nm with 9-ns pulses. In order to partially average spatial and temporal variations of the laser intensity, three successive pulses were applied to the electrode. For this study, power densities of 25 and 70  $\text{MW}/\text{cm}^2$  were utilized. Fracturing procedures were as described previously.<sup>16,17,22,23</sup> Fractured surfaces were created in situ by breaking a GC microelectrode flush with the surface of the embedding epoxy (Eccobond 55, Emerson and Cuming, Inc., Woburn, MA). Electrochemical measurements were taken immediately after fracturing. Heat treatment procedures were similar to those of Fagen et al.<sup>20</sup> Rate constant and capacitance data were obtained

(25) Engstrom, R. C.; Strasser, V. A. *Anal. Chem.* 1984, 56, 136-141.  
(26) Alsmeyer, Y. W.; McCreery, R. L. *Anal. Chem.* 1991, 63, 1289-1295.

(27) Alsmeyer, Y. W.; McCreery, R. L. *Langmuir* 1991, 7, 2370-2375.  
(28) Kazee, B.; Weisshaar, D. E.; Kuwana, T. *Anal. Chem.* 1985, 57, 2739-2740.

(29) Bodalbhaj, L.; Brajter-Toth, A. *Anal. Chim. Acta* 1990, 231, 191.  
(30) Gewirth, A.; Bard, A. J. *J. Phys. Chem.* 1988, 92, 5563.  
(31) Chang, H.; Bard, A. J. *J. Am. Chem. Soc.* 1990, 112, 4598.  
(32) Chang, H.; Bard, A. J. *J. Am. Chem. Soc.* 1991, 113, 5588.  
(33) Bowling, R.; Packard, P.; McCreery, R. L. *J. Am. Chem. Soc.* 1989, 111, 1217.

(34) Bowling, R.; McCreery, R. L.; Pharr, C. M.; Engstrom, R. C. *Anal. Chem.* 1989, 61, 2763.

(35) Snyder, S. R.; White, H. S.; Lopez, S.; Abruna, H. D. *J. Am. Chem. Soc.* 1990, 112, 1333.

(36) Hu, C. Z.; Feng, L.; Andrade, J. D. *Carbon* 1988, 26, 543-555.  
(37) Elings, V.; Wudl, F. *J. Vac. Sci. Technol. A* 1988, 6 (2), 412-414.  
(38) Brown, N. M. D.; You, H. X. *J. Mater. Chem.* 1991, 310, 127-138.  
(39) Wang, J.; Martinez, T.; Yaniv, D. R.; McCormick, L. D. *J. Electroanal. Chem.* 1990, 278, 379-386.

(40) Wang, J.; Martinez, T.; Yaniv, D. R.; McCormick, L. D. *J. Electroanal. Chem.* 1991, 313, 120-140.

(41) Freund, M. S.; Brajter-Toth, A.; Cotton, T. M.; Henderson, E. R. *Anal. Chem.* 1991, 63, 1047-1049.

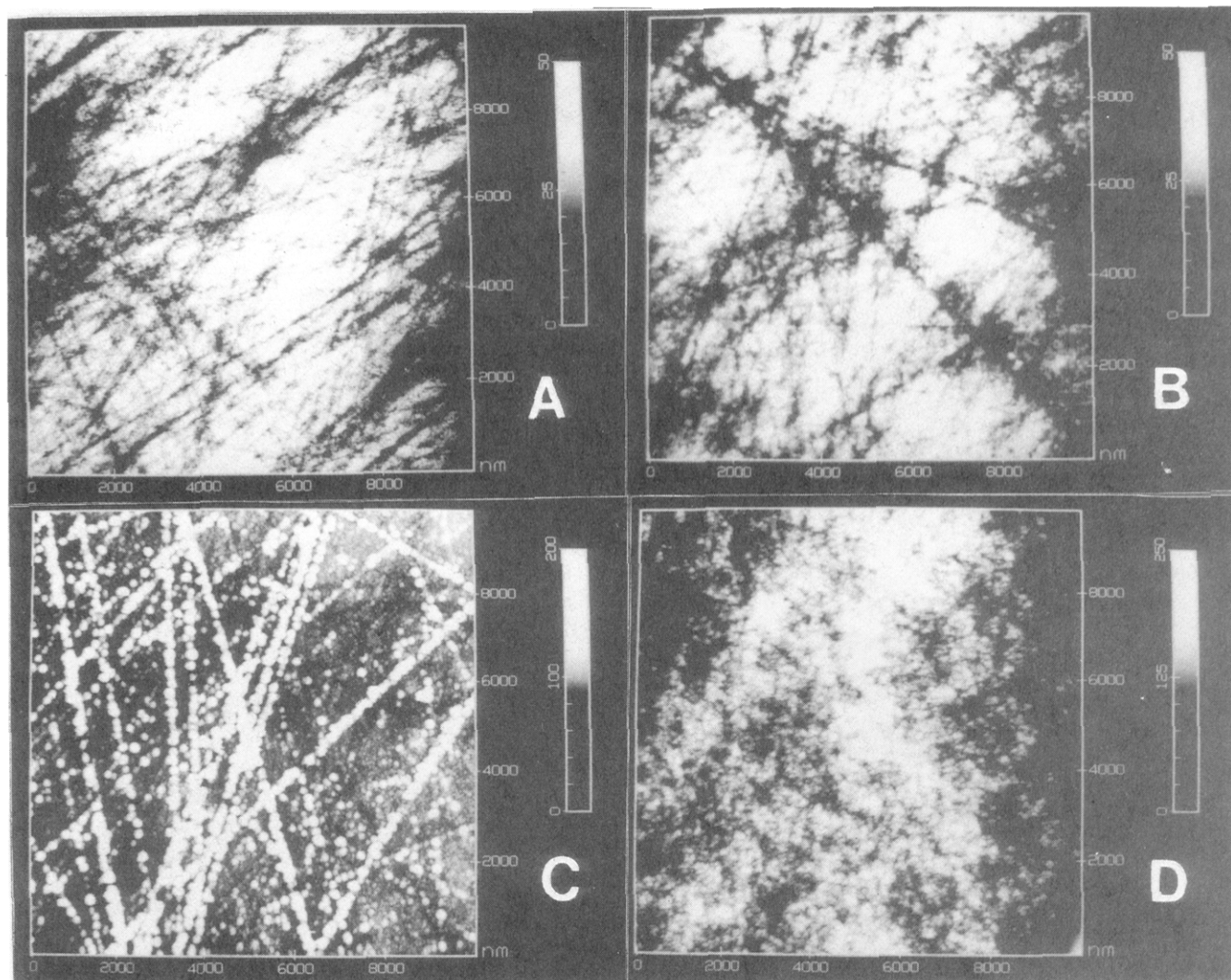


**Figure 1.** Images, 10 000 nm (full-scale  $x$  and  $y$ ), of GC electrodes after different pretreatment conditions: (A) polished GC,  $z$  scale 0–50 nm; (B) polished/laser-activated (25 MW/cm<sup>2</sup>) GC,  $z$  scale 0–50 nm; (C) polished/laser-activated (70 MW/cm<sup>2</sup>) GC,  $z$  scale 0–200 nm; (D) fractured GC,  $z$  scale 0–250 nm.

on a polished surface first and then this surface was removed from solution and deactivated by exposure to ambient air for ~12 h. After electrochemical kinetics and capacitance were again observed, the same surface was then heat treated and the last set of electrochemical data was obtained. Vacuum heat treatment (VHT) was carried out in an UHV chamber at  $10^{-8}$ – $10^{-9}$  Torr. GC disks were mounted on a sample probe tip, and the temperature was raised by ohmic heating. Heating and temperature sensing occurred on the back side of a GC disk electrode (1.5 mm thick), such that a 700 °C temperature was achieved 1–2 h. Heat-treated electrodes were exposed to ambient air for ~30 s while being inserted into the Teflon cell and bathed in analyte solution.

Highly oriented pyrolytic graphite (HOPG) was obtained from Arthur Moore (Union Carbide, Parma, OH). HOPG electrodes were cleaved with adhesive tape or with a razor blade as described previously.<sup>9,10</sup>

**Electrochemical Measurements.** Electrode areas were determined by chronoamperometry on a 5-s time scale in 1 mM Fe(CN)<sub>6</sub><sup>4-/3-</sup> in 1 M KCl. Linear sweep cyclic voltammetry experiments and  $k^0$  determination were performed as described previously<sup>9,10,18,24</sup> utilizing a function generator (Tektronix Inc., Beaverton, OR) and an Advanced Idea Mechanics (Columbus, OH) potentiostat. Differential capacitance measurements were performed by the method of Gileadi<sup>42,43</sup> and described by us previously<sup>9,17,18,23</sup> using a 100-Hz, 20-mV peak-to-peak triangle

wave centered at 0.0 V. All reported  $C^0$  values are normalized to the projected electrode area, as determined from chronoamperometry. All potentials stated are relative to the Ag/AgCl (3 M NaCl) electrode. Simulated voltammograms were calculated with the finite difference approach, and the computer program was provided by Dennis Evans,<sup>44</sup> with a constant value of the transfer coefficient.

**STM Conditions.** STM images were obtained with a Nanoscope II (Digital Instruments Inc., Santa Barbara, CA). Most images were obtained with electrochemically etched 0.01-in.-diameter tungsten wire tips, as recommended by the manufacturer. Mechanically cut Pt/Ir (80/20) tips (Digital Instruments) were also used for comparison, but no significant differences between the two types of tips were observable in the STM images at the relatively low resolution utilized for most of this work. All images were taken in ambient air, and no changes were noted in the images for many hours after initial scans.

Low-resolution images (150-nm full scale and greater) were obtained with the  $12 \times 12 \mu\text{m}$  scan head in the “height” image mode (constant current) with a bias voltage of 500 mV and a set-point current of 0.5 nA. High-resolution images (25-nm full scale and lower) were taken with a  $0.7 \times 0.7 \mu\text{m}$  scan head in the “current” image mode (constant height) with bias voltages of 20–100 mV and set-point current of 2–5 nA.

GC samples were mounted with silver paste to a thin metal plate through which the bias voltage was applied. All polished

(42) Gileadi, E.; Tshernikovski, N. *Electrochim. Acta* 1971, 16, 579–584.

(43) Babai, M.; Tshernikovski, N.; Gileadi, E. *J. Electrochem. Soc.* 1972, 119, 1018–1021.

(44) Corrigan, D. A.; Evans, D. H. *J. Electroanal. Chem.* 1980, 106, 287.

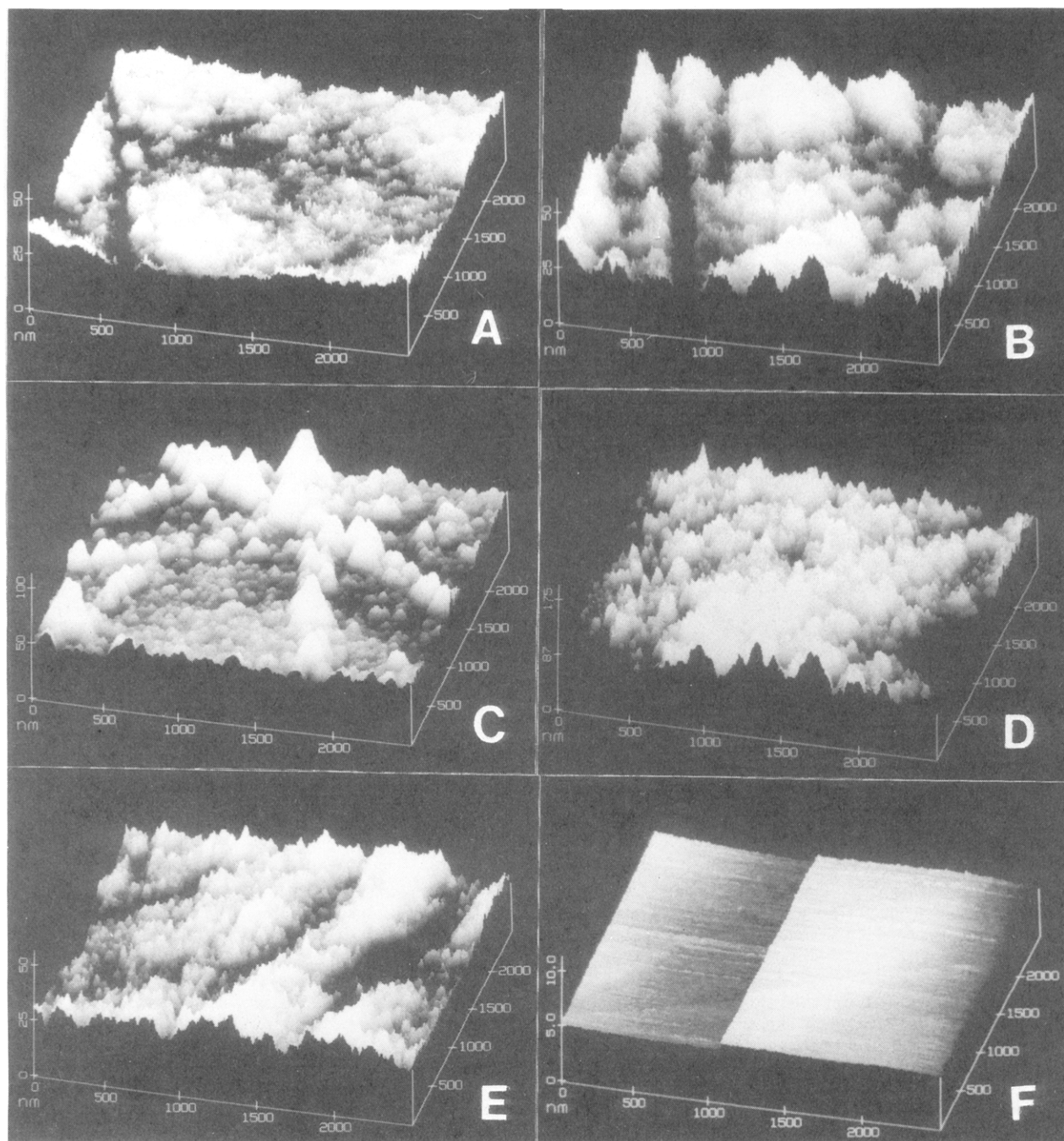


**Figure 2.** Images, 2500 nm, of electrodes under different pretreatment conditions: (A) polished GC, z scale 0–50 nm; (B) polished/laser-activated (25 MW/cm<sup>2</sup>) GC, z scale 0–50 nm; (C) polished/laser-activated (70 MW/cm<sup>2</sup>) GC, z scale 0–100 nm; (D) fractured GC, z scale 0–175 nm; (E) polished/vacuum heat treated GC, z scale 0–50 nm; (F) highly ordered pyrolytic graphite, z scale 0–10 nm.

surfaces yielded similar STM images, at the resolution employed, regardless of the electrode configuration (large disk or micro-electrode). Images of fractured surfaces were obtained on the piece fractured from the electrode rather than the electrode itself, since the electrode would not fit in the STM sample region. Different surfaces as well as several different areas of each surface were examined to obtain representative images.

## RESULTS

Figure 1 shows 10 × 10 μm survey scans of typical GC surfaces that were evaluated electrochemically. Due to image curvature which occurs with large scan areas, the images were software flattened but not smoothed or filtered. STM height scales are shown on the right sides of the plots along with the topographic grey scale; higher points appear as lighter shades. The images shown in Figure 1 are polished, polished/laser-irradiated at 25 MW/cm<sup>2</sup> (denoted P/L 25), polished/laser-

irradiated at 70 mW/cm<sup>2</sup> (denoted P/L 70), and fractured surfaces. The polished (Figure 1A) and P/L 25 (Figure 1B) surfaces appear similar in morphology, with polishing scratches visible in both images, and in height, with features not exceeding 50 nm in height. The P/L 70 (Figure 1C) and the fractured (Figure 1D) surfaces cover a greater height range and exhibit distinct morphological features. The P/L 70 surface exhibits isolated protrusions (shown as bright lines) that appear to originate from the polishing scratches that were present on the surface before laser irradiation. The fractured surface displays protrusions or nodules with diameters ranging from 50 to 300 nm. We have previously reported nodules on fractured GC electrodes based on SEM images.<sup>18</sup>

Parts A–D of Figure 2 show the same types of surfaces plotted in a 3-D perspective and on a smaller x, y scale. In

**Table I. STM Results for Seven Carbon Electrode Surfaces**

surface	samples	images	RMSR (nm)	$Z_{\max}$ (nm)
polished	6	13	$4.1 \pm 1^a$	$36 \pm 8^a$
P/L 25	4	10	$4.4 \pm 1$	$37 \pm 10$
P/L 70	6	17	$11 \pm 4$	$96 \pm 33$
fractured	5	10	$20 \pm 5$	$140 \pm 30$
P/DEAC	2	4	$4.7 \pm 1$	$38 \pm 7$
P/VHT	3	6	$4.5 \pm 0.6$	$37 \pm 4$
HOPG	1	1	0.24	2.0

<sup>a</sup> Standard deviation of RMSR and  $Z_{\max}$  for the number of images examined.

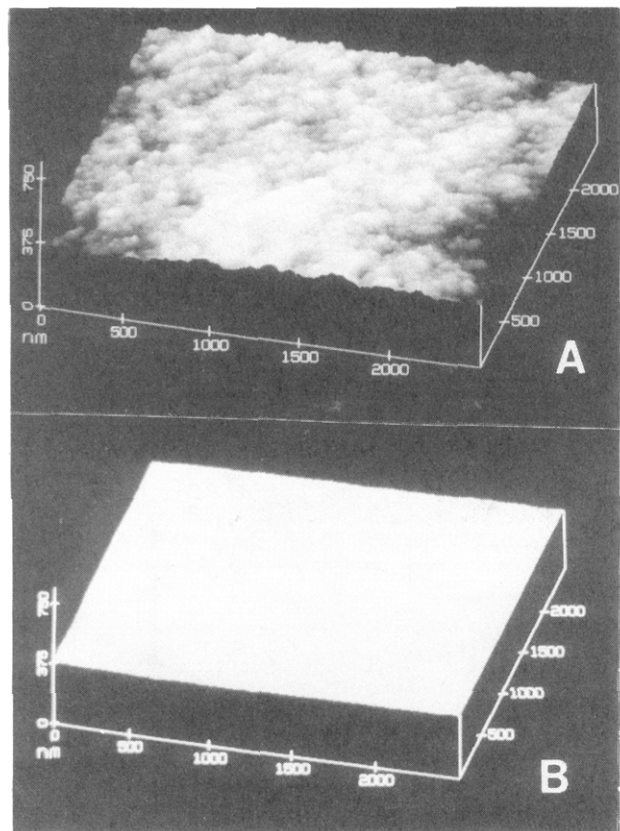


**Figure 3.** Image, 2500 nm, of (A) fractured GC plotted in a 1:1 aspect ratio compared to a similar image of (B) polished GC. z scale is 0–750 nm.

addition, images of polished/VHT (denoted P/VHT) and highly oriented pyrolytic graphite surfaces are shown in Figure 2E and F. Note the difference in z-axis scale from image to image. With this mode of image display, the differences in the surface morphologies are particularly noticeable. Polished, P/L 25, and P/VHT surfaces (Figure 2A, B, and E) appear similar, with all images employing identical height scales and exhibiting polishing scratches. The distinctive morphologies of the fractured and P/L 70 surfaces (Figure 2C and D) are apparent and will be discussed in detail below. Again, these surfaces exhibit greater height variation than the other surfaces. Figure 2F is a typical HOPG basal plane surface containing a step defect for comparison with the other images.

To provide a quantitative comparison of surface roughness, the root-mean-square roughness (RMSR) function of the Nanoscope II software was employed. RMSR is defined as the standard deviation of the height of the surface calculated from all points obtained during a given scan. For example, the image of HOPG in Figure 2F yields an RMSR of 0.24 nm, while that of fractured GC (Figure 2D) yields 20.4 nm.

Although RMSR has not been established as a rigorous quantitative measure of surface roughness, it does provide a comparison for different surfaces. An additional but less statistically useful parameter is  $Z_{\max}$ , which is the difference between the minimum and maximum surface heights.  $Z_{\max}$  and RMSR results are listed in Table I. Note that both values also include standard deviations of  $Z_{\max}$  and RMSR for the number of images indicated.

Figure 3 illustrates how the fractured surface, which exhibits the highest  $Z_{\max}$  and RMSR, would appear if plotted with a 1:1 aspect ratio between the x, y scale and the z scale. In Figure 2, and in typical STM images, the z scales are expanded in order to enhance surface features. In Figure 3, the distance on the z axis was adjusted to equal those of the x and y axes. A polished surface (from Figure 2A) is plotted similarly for comparison. Without expansion of the z-axis scale, both surfaces appear much smoother.

The unusual morphology of the fractured GC surface is shown at successively higher magnification in Figure 4. Image 4A shows the variation in nodule diameter, while 4B shows an intersection of three nodules with ca. 200-nm diameters. Images C and D show the top of the upper left nodule of Figure 4B, with a full-scale scan range of 25 nm. Note that the apparent roughness persists even on a scale of ca. 1 nm.

**Electrochemical Results.** Table II shows electron-transfer rate constants and capacitance for the six types of surfaces examined by STM. The relatively large area of several electrode types limited the scan rate to 10 V/s or less, so rate constants above 0.1 cm/s are lower limits of the true values. As noted by several authors,<sup>12,13,17</sup> the variability of  $k^\circ$  for  $\text{Fe}(\text{CN})_6^{4-/3-}$  on polished GC is quite large due to variations in cleanliness but is often in the range of  $10^{-3}$ – $10^{-2}$  cm/s. The  $k^\circ$  values obtained here are somewhat higher than typical, but do show a large standard deviation (50%) typical of polished surfaces.

Laser activation at either 25 or 70 MW/cm<sup>2</sup> or fracturing led to reliably large  $k^\circ$  values. Since the  $\Delta E_p$ 's for these surfaces were near the reversible limit of 57 mV,  $k^\circ$  determinations based solely on  $\Delta E_p$  are of limited accuracy. Figure 5 shows a comparison of the experimental voltammogram for  $\text{Fe}(\text{CN})_6^{4-/3-}$  at a fractured GC surface and a simulated response for  $k^\circ = 0.40$  and  $\nu = 10$  V/s. A  $k^\circ$  of 0.40 was the lowest which yielded a good fit to the experiment, so a  $k^\circ$  estimate of  $>0.4$  cm/s is reliable in this case. The aberrant background on the experimental voltammogram is due to the differences in the background current between the  $\text{Fe}(\text{CN})_6^{4-/3-}$  voltammogram and that obtained in supporting electrolyte, leading to inaccurate background subtraction. The background current on activated GC varies with time, making background subtraction incomplete. A more rigorous investigation of  $\text{Fe}(\text{CN})_6^{4-/3-}$  kinetics has been performed on these surfaces at scan rates which yielded a more reliable rate constant of 0.5 cm/s.<sup>17</sup> The fractured GC and the P/L 70 surfaces exhibited rate constants at least 6 times greater than that of the initial polished electrode ( $>0.4$  vs 0.060 cm/s). The rate constant value for the P/L 25 electrode is larger than that of the original polished surface by more than a factor of 5 ( $>0.3$  vs 0.060 cm/s). Recall that although the STM data show that the fractured and P/L 70 surfaces possess distinct morphologies with high  $Z_{\max}$  and RMSR values, the morphology and the  $Z_{\max}$  and RMSR values of the P/L 25 surface are very similar to those acquired for the polished surface.

Finally, the P/VHT surfaces yielded rate constant values similar to the polished surface. These results are consistent with those of Kuwana et al.<sup>20</sup> The  $\Delta E_p$  for  $\text{Fe}(\text{CN})_6^{4-/3-}$  at 10 V/s increased from 98 to 230 mV upon deactivation in ambient air, but after heat treatment, reactivation of the

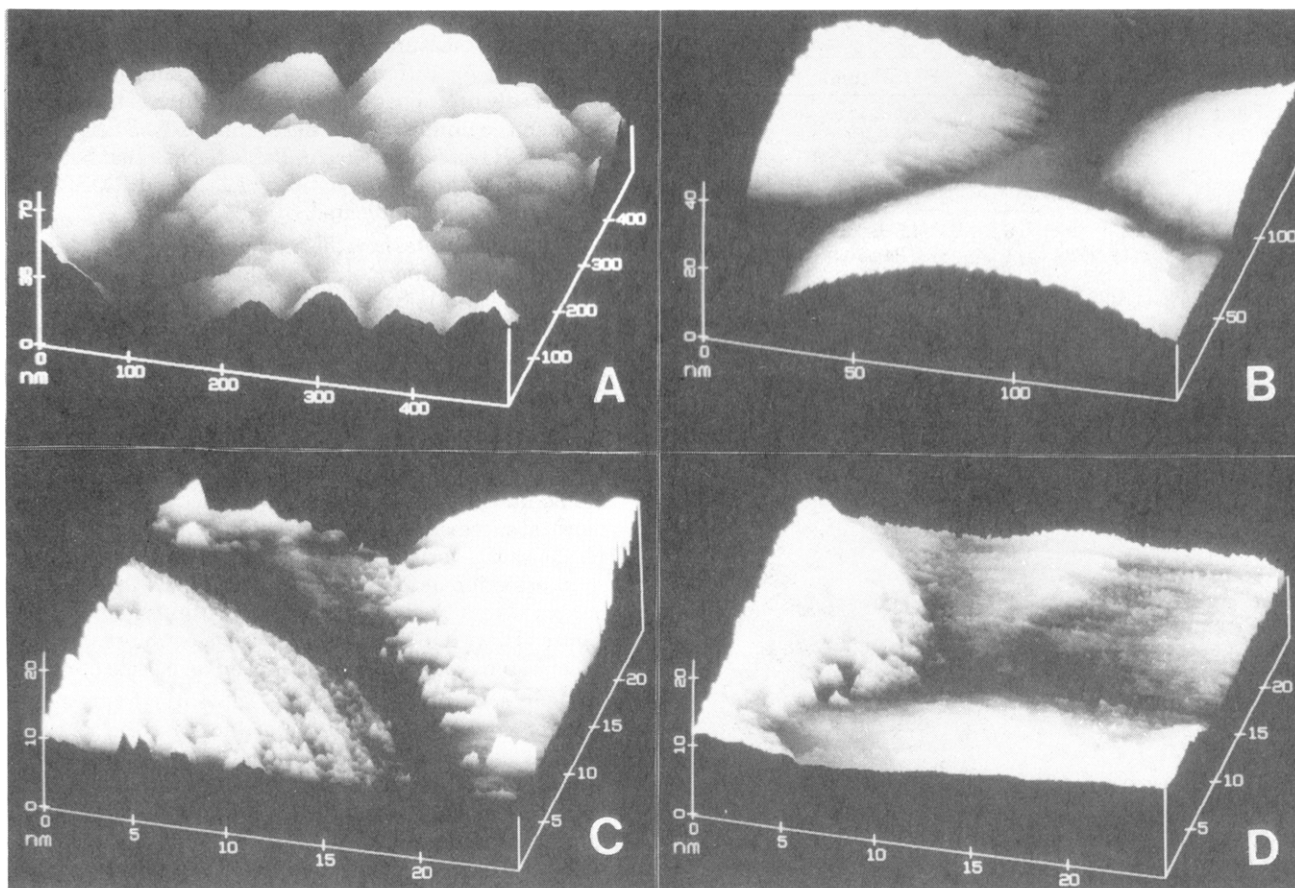


**Figure 4.** Fractured GC under higher resolution conditions: (A) 500-nm scan with z scale 0–70 nm; (B) 200-nm scan with z scale 0–40 nm; (C) 25-nm scan with z scale 0–20 nm; (D) 25-nm scan with z scale 0–20 nm. Images C and D were acquired at the upper left corner of sample in image B.

**Table II. Electrochemical Results**

surface	RMSR (nm) <sup>a</sup>	$\Delta E_p$ (mV) <sup>b</sup>	$k^\circ$ of $\text{Fe}(\text{CN})_6^{4-/3-}$ (cm/s)	$C^\circ$ <sup>c</sup> ( $\mu\text{F}/\text{cm}^2$ )	$N^d$
polished	4.1	$98 \pm 29$	$0.06 \pm 0.03$	$33 \pm 6$	14
P/L 25	4.4	$71 \pm 12$	$>0.3$	$34 \pm 7$	4
P/L 70	11.0	$62 \pm 6$	$>0.4$	$120 \pm 31$	3
fractured	20.0	$58 \pm 4$	$>0.4$	$75 \pm 16$	4
P/DEAC	4.7	$232 \pm 42$	$(8.4 \pm 4) \times 10^{-3}$	$15 \pm 2$	3
P/VHT	4.5	$96 \pm 13$	$0.065 \pm 0.020$	$40 \pm 5$	3
HOPG <sup>e</sup>	0.24	$>1200$	$<1 \times 10^{-6}$	$<1.0$	

<sup>a</sup> Values repeated from Table I. <sup>b</sup>  $\nu = 10$  V/s. <sup>c</sup> Based on chronoamperometric area. <sup>d</sup> For electrochemical results, not RMSR. <sup>e</sup> Values from ref 8.

electrode occurred to a level equal to or greater than that of the initial polished surface.

Differential capacitance ( $C^\circ$ ) values are also shown in Table II. The fractured and P/L 70 surfaces exhibit higher  $C^\circ$  values than the other surfaces as well as the largest variation in capacitances.  $C^\circ$  values for polished, P/L 25, and VHT surfaces are similar. Note that deactivation decreased  $C^\circ$  by a factor of 2 while decreasing  $k^\circ$  of  $\text{Fe}(\text{CN})_6^{4-/3-}$  by a factor of 7 from the original polished surface. The significant influence of adsorbed airborne impurities on the activity of GC is illustrated in these decreases in  $k^\circ$  of  $\text{Fe}(\text{CN})_6^{4-/3-}$  and  $C^\circ$  from the polished to the P/DEAC surface. We have observed that exposure of a polished GC surface to air for even a few seconds leads to lower rate constants for  $\text{Fe}(\text{CN})_6^{4-/3-}$ . As noted in the Experimental Section, great care was taken to ensure that a drop of water remained on the electrode surface during handling after polishing and sonication. Also note that the marked decrease in electro-

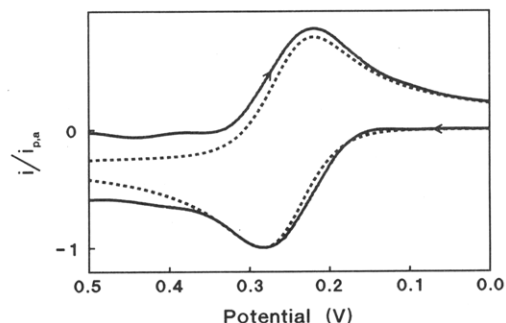


**Figure 5.** Experimental (solid line) and simulated (dashed line) cyclic voltammograms of 1 mM  $\text{Fe}(\text{CN})_6^{4-/3-}$  on fractured GC in 1 M KCl at  $\nu = 10$  V/s. Simulation assumed  $\alpha = 0.5$ ,  $k^\circ = 0.4$  cm/s, and  $D_{\text{red}} = 6.32 \times 10^{-6}$  cm<sup>2</sup>/s.

chemical activity through exposure to ambient conditions followed by reactivation via VHT was not accompanied by significant morphological changes.

## DISCUSSION

The STM results discussed above are relevant to two issues regarding GC surface structure: morphological characteristics of GC electrodes under different pretreatment conditions and the quantitation of microscopic roughness and electrochemical activity. Previous insight on the morphology of GC electrodes prepared according to the methods reported here has originated from scanning electron microscopy.<sup>18,28,29</sup> Although SEM provides the necessary magnification for elementary image analysis, the resolution (particularly in the vertical direction) is poor compared to STM. Electrode roughness has been investigated previously by indirect means such as

**Table III. Effect of Laser Power on Surface Protrusions for P/L Surfaces**

power density (MW/cm <sup>2</sup> )	no./ image <sup>a</sup>	% coverage <sup>b</sup>	av ht (nm) <sup>c</sup>
25	0		
30	0.5	1.3	20
40	2	4.5	20
50	5.6	10	26
70	12	42	57

<sup>a</sup> Average number of protrusions per 10 × 10 μm scan image based on four images. <sup>b</sup> Percentage of the total area in a 10 × 10 μm scan covered by protrusions. <sup>c</sup> Average height of protrusions for a given power density.

adsorption and differential capacitance measurements.<sup>17,18,20,29,45</sup> One would expect that  $k^\circ$  and capacitance should scale with microscopic area of the electrode, all else being equal, and that activation may be caused in part by increases in surface roughness.

At first glance, there does appear to be a correlation between the STM determined RMSR,  $k^\circ$ , and  $C^\circ$ . The surfaces with the largest  $k^\circ$  and  $C^\circ$  (fractured and P/L 70) also exhibit the highest RMSR. Further consideration, however, reveals that the correlation is inconsistent. Polished, P/L 25, P/VHT, and P/DEAC surfaces have RMSR values which vary by less than 15%, while their  $k^\circ$ 's vary by at least a factor of 50. Laser activation at 25 MW/cm<sup>2</sup> leads to an increase in  $k^\circ$  of more than a factor of 5, yet the RMSR increase is only ~7%. These results are consistent with those presented previously based on SEM and phenanthrenequinone (PQ) adsorption.<sup>17,18</sup> They also confirm the conclusions from other laboratories that changes in microscopic roughness are not sufficient to explain the effects of activation procedures on kinetics and adsorption.<sup>29,45</sup> Large increases in  $k^\circ$  occurred upon laser activation with only minor changes in morphology and microscopic area as determined from phenanthrenequinone adsorption.<sup>17</sup> In the case of the fractured surface, the higher RMSR is due to nodules and obviously implies higher roughness. On the basis of PQ adsorption, the fractured surface has about twice the microscopic area of the polished or P/L 25 surfaces.<sup>18</sup> Thus variations in roughness could reasonably account for a factor of ~2 in  $k^\circ$ , but the major source(s) for  $k^\circ$  variation must lie elsewhere.

We have previously attributed  $k^\circ$  increases caused by laser activation to the removal of adsorbed impurities.<sup>17</sup> This conclusion is reinforced by the VHT experiments of Fagan et al.<sup>20</sup> and Stutts et al.,<sup>21</sup> repeated here with the addition of STM characterization. Deactivation and subsequent VHT led to minimal changes in RMSR from the polished surface yet yielded large variation in  $k^\circ$ . As expected for impurity adsorption, the capacitance decreases for the P/DEAC surface. The low  $C^\circ$  values reported by Fagan et al. were not observed here, probably due to the very different frequency domains used in the capacitance measurements. Taken together with results from other laboratories, the STM and electrochemical results strongly support the conclusion that the major factor controlling  $k^\circ$  for Fe(CN)<sub>6</sub><sup>4-/3-</sup> on GC is surface cleanliness, with surface roughness playing a minor role. Stated semi-quantitatively, roughness accounts for a factor of ~2 in observed  $k^\circ$  on GC, while surface cleanliness can affect  $k^\circ$  for Fe(CN)<sub>6</sub><sup>4-/3-</sup> by factors as large as several hundred.

The second major issue addressed by the STM examination deals with the morphological effects of various pretreatments, particularly laser activation. The unique features of the fractured surface are obvious from SEM or STM. The increased roughness leads to increases in capacitance and  $k^\circ$

for fractured surfaces compared to P/L 25 surfaces, but these effects are not large (a factor of ~2). The major consequence of in-situ fracturing with regard to  $k^\circ$  enhancement is the avoidance of impurity adsorption. At least at the resolution employed here, the morphological differences between fractured and polished surfaces do not appear to have major consequences for observed kinetics. The effect of polishing is to flatten the tops of nodules, yielding the surfaces of Figures 1A and 2A, accompanied by the undesired consequence of impurity adsorption.

While laser activation at 25 MW/cm<sup>2</sup> had no observable morphological effects at the resolution employed, higher power densities led to qualitatively distinct features. The protrusions apparent in Figure 2C formed along polishing scratches (apparent in Figure 1C). Atomic force microscope images of these features were very similar in appearance, indicating that they are not an artifact due to multiple tunneling points as the STM tip negotiates the scratches. The density and height of the protrusions increase with power density (Table III). At 30 MW/cm<sup>2</sup> and lower, they are very infrequent or not present, while at 70 MW/cm<sup>2</sup>, they cover more than 40% of the surface. We have reported previously that significant excursions in  $C^\circ$  and PQ adsorption occur at powers above 30 MW/cm<sup>2</sup><sup>18</sup> and that a surface temperature simulation predicts that local melting should occur with a threshold between 30 and 40 MW/cm<sup>2</sup> for GC.<sup>46</sup> It is likely that the protrusions are caused by local melting, perhaps followed by expansion of heated, entrapped gases. The localization of protrusions on polishing scratches may result from the lower reflectivity inside the scratches, resulting in more efficient coupling of the laser light into the GC. In addition, the thermal conductivity near scratches could be different, leading to localized temperature variations.

The high-resolution images of the top of a nodule on the fractured surface (Figure 4C and D) are not of sufficient resolution to image individual atoms. The apparent roughness, which is on a much smaller scale than that shown in Figures 1 and 2, could be due to genuine morphological features or to variations in electronic interactions between the tip and the surface during scanning. Although these features are reproducible, it is not yet clear what they represent. A few reports here appeared on high-resolution STM of disordered carbon materials.<sup>36-38</sup> Atomic resolution was achieved, although the polishing procedures employed leaves some doubt about the condition of the surface. Unusual arrangements of carbon atoms were observed, perhaps because of deviations of the electronic structure of disordered carbons from that of HOPG. The high-resolution images on the fractured surface obtained here are of value because the fractured surface is unmodified by polishing and should be more representative of bulk structure. Attempts to obtain atomic scale images of the fractured surface are currently being made.

## SUMMARY

The foremost conclusion drawn from the correlation of electrochemical properties with STM images is that some phenomenon other than surface roughening is responsible for increases in electrode activity toward Fe(CN)<sub>6</sub><sup>4-/3-</sup> upon laser or VHT activation. This statement is especially apparent with comparison of the polished and P/L 25 surfaces. Results show that laser activation at 25 MW/cm<sup>2</sup> causes no changes in capacitance and roughness, but causes a drastic increase in activity as evidenced by the heterogeneous rate constant for Fe(CN)<sub>6</sub><sup>4-/3-</sup>. These results are consistent with a mech-

anism in which electrode activity is determined by exposure of active sites and activation occurs through a cleaning process. STM images of polished, P/L 25, P/VHT, and P/DEAC electrodes show them to be similar in morphology, indicating that any changes induced by laser activation at low power densities and vacuum heat treatment at temperatures of  $\sim 700$  °C are minimal. Fractured and P/L 70 surfaces exhibit distinct morphologies with a large amount of roughness and some variability in electrochemical behavior. Morphological characteristics of the P/L 70 surface are attributed to possible melting of the GC substrate at high laser power densities, beginning at 30–40 MW/cm<sup>2</sup>. Investigation of these surfaces with AFM and with STM at higher resolution is currently underway.

#### ACKNOWLEDGMENT

The authors thank Robert S. Robinson for assistance with STM techniques and initial STM examinations of GC surfaces and Roy Tucker for assistance with UHV heat treatment. The work was supported by the Air Force Office of Scientific Research, an ACS Analytical Division Fellowship sponsored by Eli Lilly and Co. to C.A.M., and an Amoco Foundation Doctoral Fellowship to M.T.M.

RECEIVED for review July 27, 1992. Accepted December 30, 1992.